Supplemental Material:
Supplemental Methods and Supplemental Figures

Torsional Stiffness of Extended and Plectonemic DNA

Xiang Gao[1,2], Yifeng Hong[3], Fan Ye[1,2], James T. Inman[1,2], and Michelle D. Wang[1,2,*]

[1]Howard Hughes Medical Institute, [2]Department of Physics & LASSP, [3]Department of Electrical and Computer Engineering, Cornell University, Ithaca, NY 14853, USA.

Supplemental Methods

S1. DNA template preparation

Each DNA template is composed of a middle segment of 12,688 bp for data in the main figures or 12,667 bp for the data in Fig. S4, and is flanked by ~500 bp multi-labeled tethering adaptor at each end. The 12,688 bp middle segment was PCR-amplified from λ DNA. The 12,667 bp middle segment contains 64 repeats the 601 nucleosome positioning element and was constructed as previously described[1]. Both templates are flanked by the same multi-labeled adaptors labeled with either biotin or digoxigenin[1].

S2. Angular optical trap

The AOT is able to precisely manipulate the extension and twist of a single DNA molecule and simultaneously measure the force and torque on DNA[2,3]. The AOT is a flexible and versatile instrument, permitting a variety of feedback modes of operation[3,4]. In an AOT, a

nanofabricated quartz cylinder is trapped by a focused linearly polarized laser. The cylinder is fabricated so that the extraordinary axis is perpendicular to the cylinder axis. When trapped, the cylindrical axis is oriented along the direction of light propagation and the extraordinary axis of the cylinder is aligned with the polarization direction. When the cylinder experiences a torque τ from the DNA attached on the bottom surface of the cylinder, the cylinder rotates around its cylindrical axis by an angle θ according to $\tau = \tau_0 \sin(2\theta)$.

The force and torque are controlled separately via independent modulation of the trap height and the input laser polarization. When an external torque is applied to the trapped cylinder, the spin angular momentum of the light transmitted through the cylinder is changed and the transmitted light becomes elliptically polarized. Thus, the optical torque imparted onto the cylinder is detected via the angular momentum of the transmitted light[3]. The detection method is exceedingly direct and distinguishes the AOT from other torque detection methods.

For long DNA templates (~12.7 kbp) used in this study, torsional measurements must be performed over an extended axial distance (from 0 to 4 μm away from the coverslip surface) using the AOT. Therefore, we have optimized the AOT to allow for accurate torque and force measurements over this broad axial distance via systematic optical alignment and rigorous calibrations[1].

S3. Nanofabrication of quartz cylinders

The protocols for the nanofabrication and functionalization of the quartz cylinders used in this work were based on those previously described[1,2] with the following modifications to improve cylinder homogeneity by using a deep UV etching technique (Fig. S1a). A 4-inch X-cut quartz wafer (Precision Micro-Optics) was first washed by hot piranha and then functionalized by (3-aminopropyl) trimethoxysilane (APTMS) via molecular vapor deposition. The photoresist patterning step was based on deep ultraviolet (DUV) lithography with positive photoresist UV1400-1.4 (Rohm and Haas Electronic Materials LLC) along with developable anti-reflection coating DS-K101, which enabled the fabrication of cylinders with smaller diameters. A reactive

ion etching process with high-selectivity etching chemistry (45 sccm CHF_3, 15 sccm Ar, 50 mTorr, 200 W) was used to etch the quartz wafer, providing ~ 1 μm height quartz cylinders with 87.5° side-wall angle and a smooth sidewall. After removing the photoresist with Microposit Remover 1165, the cylinders were manually cleaved off using a razor blade. Finally, the cylinders were collected and then coupled to streptavidin (Agilent).

The resulting quartz cylinders have the following properties measured from the SEM images (all parameters expressed as mean ±SD): 443 ± 17 nm top diameter, 545 ± 25 nm bottom diameter, and 1133 ± 29 nm height (Fig. S1b).

S4. Data acquisition and analysis

Microscope coverslips and slides used to make single-molecule sample chambers were cleaned by 95% ethanol. A cleaned coverslip and a glass slide were assembled into a microfluidic sample chamber formed using inert silicone high vacuum grease and stored in a clean plastic container for 24 hours or more before use.

Prior to an experiment, a sample chamber was first incubated with 5 ng/μL anti-digoxigenin for 20 min (Vector Laboratory, MB-7000). The surface was then passivated by flushing the chamber with 10 mg/mL β-casein (Sigma, C6905) in PBS and incubated for 20 min. To form DNA tethers, the surface was incubated with 1 pM DNA in PBS with 1 mg/mL β-casein for 15 min. The chamber was then flushed thoroughly to remove free DNA molecules, and then incubated with cylinders for 15 min. The chamber was flushed by a buffer containing both monovalent and divalent ions (10 mM Tris-HCl pH 8.0, 50 mM KCl, 50 mM NaCl, 3 mM $MgCl_2$, 1 mM ATP, 0.1 mM EDTA, and 1.5 mg/mL β-casein). The same buffer has been previously used in our topoisomerase assays[1]. All experiments were carried out in this buffer on the AOT in a soundproof cleanroom, which was maintained at a temperature of 23°C.

DNA elasticity properties are known to be sensitive to the buffer conditions. To determine the bending persistence length of DNA A under the buffer condition used here, we carried out a

DNA stretching experiment using the AOT. This experiment used a DNA molecule with the same length as that for the winding experiments, except that the DNA contained a single-labelled tag at each end and thus could not be torsionally constrained. Using the AOT, the DNA molecule was stretched axially. The resulting force-extension curve was used to determine A using a method similar to that previously described[5]. We found that $A = 43$ nm.

We first carried out the winding experiments under constant force, similar to those previously described[1,6-10]. In Fig. 1a, a DNA molecule was torsionally constrained to the surface of an anti-dig coated coverslip and to the bottom surface of a streptavidin-coated quartz cylinder. The DNA was then held under a fixed force by the AOT. A PID feedback loop was used to modulate the piezo position to clamp the force on the DNA molecule as the DNA molecule was twisted by rotation of the trapped cylinder at a constant 1 turns/s (for 0.25 pN, 0.5 pN, 1 pN, and 2 pN) or 2 turns/s (for 5 pN). Data were collected at 400 Hz and smoothed with a sliding window of 4 s for torque and 1 s for force. We fit the torque data in the pre-buckling region to determine the torsional stiffness of the DNA for data at 0.5 pN, 1 pN, and 2 pN. The buckling transition at 0.25 pN is less obvious, we fit the data within 60 % of pre-buckling region.

We implemented the constant-extension method on the AOT by modulating the piezo position along the axial direction of the trap. Specifically, the extension of DNA was determined from the axial position of the piezo and the axial displacement of the cylinder from the trap center, and a software-based PID controller tuned the piezo position to maintain the extension at the set value. In the experiments shown in Fig. 1b, we introduced ± 20 turns to the DNA and measured the resulting force and torque while maintaining a constant extension. The force and torque were measured as function of turns at four different extensions (500, 1000, 2000, and 2800 nm). At these extensions, the predicted forces by Bouchiat et al.[11] are 0.017, 0.036, 0.92 and 0.21 pN, respectively. Data were collected at 400 Hz and smoothed with a sliding window of 2 s for torque and force. We linearly fit the torque data within ± 10 turn (supercoiling density = ± 0.008) to obtain the effective torsional moduli at these extensions. This range should correspond to the pre-buckling region of the data (see Supplemental Methods S9). In Fig. 2, for

each extension, the force corresponds to the mean force in the fitting range, and the error bars are the minimal and maximal force in the fitting range.

S5. Conversion from torque slope to twist persistence length

C_{eff} may be obtained from the torque slope k_θ of a torque versus rotational angle θ plot:

$$\tau = k_\theta \theta = \frac{k_B T C_{\mathrm{eff}}}{L} \theta, \tag{S1}$$

where L is the DNA contour length. Therefore,

$$C_{\mathrm{eff}} = \frac{k_\theta L}{k_{\mathrm{B}} T}. \tag{S2}$$

P may be obtained in a similar fashion.

S6. Force offset

In an AOT, the zero-force reading from the force detector can in principle be obtained by the reading at which a free (untethered) quartz cylinder is trapped. However, this zero-force reading is specific to each cylinder, as different cylinders have slightly different dimensions. For a cylinder tethered to the surface via a DNA molecule, we approximate the zero-force condition by bringing the cylinder to near the surface of the coverslip to determine the zero-force reading. Strictly speaking, this condition is not truly zero force, because a DNA molecule has a finite hydrodynamic radius, creating an excluded volume that prevents the cylinder from reaching the surface. Thus, the zero-force reading using this method may have a small force offset, on the order of 0.01 pN, from the actual zero-force. For most applications, the desired force is much larger than this force offset. However, for applications requiring extremely low forces, this force accuracy no longer suffices. For the extremely low-force applications, we instead determine the correct zero-force reading of the force-detector using the measured DNA extension and the well-established force-extension relation for DNA under no torsion. The small

force offset between the two methods is then identified and removed from the measured force data.

S7. Pre-buckling – Numerical calculations of $C_{\mathrm{eff}}(F)$ using the Bouchiat-Mézard (BM) model

Bouchiat and Mézard (BM) have developed a theory for torsional properties of DNA[12,13]. Here we seek to find numerical solutions of the effective twist persistence length following the BM theory. In their rod like chain (RLC) model, a given configuration of a supercoiled DNA molecule is parameterized by Euler angles $\theta(s)$, $\phi(s)$, and $\psi(s)$, where s is the arc length along the DNA molecule. The bending energy, twisting energy, and stretching energy of the RLC under force F are given by:

$$\frac{E_{\mathrm{bend}}}{k_{\mathrm{B}}T} = \frac{A}{2}\int_0^L \left(\frac{d\hat{t}}{ds}\right)^2 ds = \frac{A}{2}\int_0^L \left(\dot{\phi}^2 \sin^2\theta + \dot{\theta}^2\right) ds \tag{S3}$$

$$\frac{E_{\mathrm{twist}}}{k_{\mathrm{B}}T} = \frac{C}{2}\int_0^L \Omega_3^2 ds = \frac{C}{2}\int_0^L \left(\dot{\psi} + \dot{\phi}\cos\theta\right)^2 ds \tag{S4}$$

$$\frac{E_{\mathrm{stretch}}}{k_{\mathrm{B}}T} = -\int_0^L \frac{F\cos\theta}{k_{\mathrm{B}}T} ds \tag{S5}$$

where $\hat{t}$ is the unit vector tangent to the chain, and Ω_3 is the rotational angle per unit length along the direction tangent to the chain. A and C are bending and twisting persistence length of DNA respectively, F is the stretching force, and $k_{\mathrm{B}}T$ is the thermal energy. The total energy of the rod like chain is the sum of the bending, twisting, and stretching energies:

$$E_{\mathrm{RLC}} = E_{\mathrm{bend}} + E_{\mathrm{twist}} + E_{\mathrm{stretch}}. \tag{S6}$$

Since there is a close analogy between the functional integral of the partition function

$$Z(\theta_1, \phi_1, \psi_1, s_1 | \theta_0, \phi_0, \psi_0, s_0) = \int D(\theta, \phi, \psi) \exp\left(-\frac{E_{\mathrm{RLC}}}{k_{\mathrm{B}}T}\right) \tag{S7}$$

and the Feynman amplitude

$$\langle \theta_1, \phi_1, \psi_1, s_1 | \theta_0, \phi_0, \psi_0, s_0 \rangle$$

$$= \int D(\theta, \phi, \psi) \exp\left(-i \int_{t_0}^{t_1} dt L(t) \right)$$

$$= \langle \theta_1, \phi_1, \psi_1 | \exp\left(-i(t_1 - t_0)\widehat{H}\right) | \theta_0, \phi_0, \psi_0 \rangle, \quad \text{(S8)}$$

Bouchiat and Mézard thus convert the calculation of the partition function into an eigenvalue problem of the Schrödinger equation of a quantum mechanical symmetric top. They first find the Hamiltonian operator of the DNA energy. We omit the derivations and only show the result here. The Hamiltonian as a function of force (F) and torque (τ) has the form

$$\widehat{H} = -\frac{1}{2\,sin\,\theta}\frac{\partial}{\partial\theta}\left(sin\,\theta\,\frac{\partial}{\partial\theta}\right) + \left[-\frac{FA}{k_B T}\cos\theta - \frac{\tau^2}{2(k_B T)^2}\cdot\frac{1-cos\,\theta}{1+cos\,\theta}\right]. \quad \text{(S9)}$$

However, Bouchiat and Mézard note that this Hamiltonian leads to pathological results. Therefore, they discretize the chain by adding a cut-off factor to the potential to regularize the potential operator, and the new Hamiltonian is written as follows:

$$\widehat{H} = -\frac{1}{2\,sin\,\theta}\frac{\partial}{\partial\theta}\left(sin\,\theta\,\frac{\partial}{\partial\theta}\right) + \left[-\frac{FA}{k_B T}\cos\theta - \frac{\tau^2}{2(k_B T)^2}\cdot\frac{1-\cos\theta}{1+\cos\theta}\cdot\frac{I_1\left(A\sin^2\theta/b\right)}{I_0(A\sin^2\theta/b)}\right], \quad \text{(S10)}$$

where I_1 and I_0 are the modified Bessel functions of the 1st kind. b is the length used to discretize the continuous chain and was chosen to be $b = 0.14A$.

The detailed procedures of our numerical solutions are shown as follows. First, the ground state energy ϵ_0 should be obtained by solving the Schrödinger equation

$$\widehat{H}\Psi_0(\theta) = \epsilon_0\Psi_0(\theta). \quad \text{(S11)}$$

The regularized boundary conditions can be obtained as follows: substitute $\Psi(\theta)$ by its Taylor series expansion at $\theta = 0$ in the Schrödinger equation and obtain

$$2(\epsilon_0 - V)\Psi(0) + \left[\frac{\cos\theta}{\sin\theta} + 2(\epsilon_0 - V)\theta\right]\Psi'(0) + O\left(\Psi''(0)\right) = 0, \quad \text{(S12)}$$

where

$$V = -\frac{FA}{k_{\mathrm{B}}T}\cos\theta - \frac{\tau^2}{2(k_{\mathrm{B}}T)^2}\cdot\frac{1-\cos\theta}{1+\cos\theta}\cdot\frac{I_1(A\sin^2\theta/b)}{I_0(A\sin^2\theta/b)}. \tag{S13}$$

We reason that to keep the equation regular, every term should be regular when $\theta = 0$. This requires $\Psi'(0) = 0$. In a similar way, the boundary condition at $\theta = \pi$ is $\Psi'(\pi) = 0$.

Next, we numerically integrate the Schrödinger equation to obtain the wave function $\Psi(\theta)$. To perform the integration, the second-order ordinary differential equation (ODE) is converted to two first-order ODEs

$$\frac{d}{d\theta}\begin{pmatrix}\Psi\\ \mathrm{y}\end{pmatrix} = \begin{pmatrix}0 & 1\\ -2(\epsilon_0 - V) & -\cos\theta/\sin\theta\end{pmatrix}\begin{pmatrix}\Psi\\ \mathrm{y}\end{pmatrix}, \tag{S14}$$

where $\mathrm{y} = d\Psi/d\theta$. Using the initial guess $\epsilon_0 = -(FA/k_{\mathrm{B}}T)^2/3$, the wave function $\Psi(\theta)$ is integrated from each boundary ($\theta = 0$ and $\theta = \pi$) towards the center with the regularized boundary conditions: $\Psi_1'(0) = \Psi_2'(\pi) = 0$. We also set $\Psi_1(0) = \Psi_2(\pi) = 1$ for simplicity. The numerical integration is calculated by the function "odeint" in scipy, which is based on the RK45 method with a variable step size.

When the two integrals meet at $\theta_0 = \pi/2$, the values of the two wave functions are not necessarily the same; however, the two wave functions are considered to be identical if they only differ by a constant scaling factor, as such, the Wronskian determinant equals to zero, i.e.,

$$W = \begin{vmatrix}\Psi_1 & \Psi_2\\ \Psi_1' & \Psi_2'\end{vmatrix} = 0 \tag{S15}$$

To find ϵ_0 that makes $W = 0$, we minimize $|W|$ by tuning ϵ_0 until $|W| < 10^{-12}$. The minimization is done by the Nelder-Mead method.

Once the ground state energy ϵ_0 is obtained, the extension $\langle z\rangle$ and the linking number density σ of the DNA can then be calculated by the derivatives of ϵ_0:

$$\frac{\langle z \rangle}{L} = \frac{k_B T}{A} \frac{\partial \epsilon_0}{\partial F} \tag{S16}$$

$$\sigma = \frac{\tau}{k_B T} \frac{L}{A} \left[\frac{A}{C} - 2(k_B T)^2 \frac{\partial \epsilon_0}{\partial (\tau^2)} \right] \tag{S17}$$

The derivatives of ϵ_0 were numerically calculated by the finite difference method,

$$\frac{\partial \epsilon_0}{\partial f} = \frac{\epsilon_0(F+\Delta F, \tau^2) - \epsilon_0(F-\Delta F, \tau^2)}{2\Delta f} \tag{S18}$$

$$\frac{\partial \epsilon_0}{\partial (\tau^2)} = \frac{\epsilon_0(F, \tau^2+\Delta\tau^2) - \epsilon_0(F, \tau^2-\Delta\tau^2)}{2\Delta\tau^2} \tag{S19}$$

The step sizes in the differentiation are

$$\Delta F = 0.001\, k_B T/A. \tag{S20}$$

$$\tau^2 = 0.001\, (k_B T)^2. \tag{S21}$$

The effective twist persistence length should also be calculated numerically at very small turns:

$$C_{\text{eff}} = \frac{1}{k_B T} \frac{h}{2\pi} \frac{\Delta\tau}{\Delta\sigma}, \tag{S22}$$

where h is the helical pitch of DNA (3.55 nm). We use $\Delta\tau = 0.01\, k_B T$.

To verify our numerical implementation of the BM model, we first calculated the force-extension relation of DNA under zero torsion using the BM model. Previously Marko and Siggia (MS) proposed the following interpolation formula as a useful approximation to the worm-like-chain (WLC) model[14]:

$$F = \frac{k_B T}{A} \left[\frac{z}{L} + \frac{1}{4(1-z/L)^2} - \frac{1}{4} \right]. \tag{S23}$$

This interpolation formula reduces to the exact solution the low force regime, deviates from the exact model at the intermediate force region[12] and high force region[5]. In our study, the forces employed are either low or intermediate. Bouchiat et al.[11] showed that for these force

regimes, this formula may be improved to better approximate the exact solution of the BM model by including a 7th-order polynomial correction:

$$F = \frac{k_B T}{A}\left[\frac{z}{L} + \frac{1}{4(1-z/L)^2} - \frac{1}{4} + \sum_{i=2}^{7} a_i \left(\frac{z}{L}\right)^i\right], \quad \text{(S24)}$$

with a_2 = -0.5164228, a_3 = -2.737418, a_4 =16.07497, a_5 = -38.87607, a_6 = 39.49944, and a_7 = -14.17718. Therefore, Eq. S24 serves as a simple check of our numerical results of the BM model. In Fig. S2, we compare the force-extension relations obtained from our numerical results of the BM model and that from Eq. S24. We find them essentially identical.

To further validate our reproduction of the BM model, we calculated the hat curves using the same parameters as those used in Fig. 1 of the original BM model[12]. Comparison of the hat curves from our reproduction of the BM model and from the original BM model shows that they are nearly identical (Fig. S5).

Together, our reproductions of the force-extension curves and the hat curves provide validation for our technical procedures in implementing the BM model numerically.

We have also investigated how C_{eff} versus F relation of the BM model depends on model parameters (Fig. S6). As expected, the bending persistence length A affects C_{eff} primarily at the low force regime where bending fluctuations are significant, while the twist persistence length C affects C_{eff} through the entire force range.

Note that Eq. S24 is also used to convert the measured extension at zero turns to the force in constant extension experiments in Fig. 1b, Fig. 3a, and Fig. S4b. Eq. S22 has been used in Fig. 2, Fig. S4c, and Fig. S6. Equation S16 of the BM model has been used to reproduce the original data of the BM model in Fig. S5.

S8. Pre-buckling – $C_{\mathrm{eff}}(F)$ of Moroz-Nelson (MN) model

Moroz and Nelson developed a theory for the torsional stiffness of DNA under an applied force[15,16]. We briefly recap the conclusions of this MN model. To avoid the breakdown of

Fuller formula at $\theta = \pi$, instead of introducing a cutoff as Bouchiat and Mézard did, they restricted the theory to the high force regime. They solved the Hamiltonian using the perturbation theory about $\theta = 0$. The approximated expression of the effective twist persistence length of extended DNA can be written as follows

$$C_{\text{eff}} = \left(\frac{1}{C} + \frac{1}{4A} \sqrt{\frac{k_{\text{B}}T}{FA}} \right)^{-1}. \tag{S25}$$

Subsequently, Marko introduced a variation of this expression[17]:

$$C_{\text{eff}}(F) = C \left(1 - \frac{C}{4A} \sqrt{\frac{k_B T}{AF}} \right). \tag{S26}$$

We refer to this variation as the modified-modified MN (modified-MN) model.

Note that Equation S25 of the MN model has been used in Fig. 2 and Fig. S4. Equation S26 of the modified-MN model has been used in Fig. 2, Fig. 3, Fig. S3, Fig. S4, Fig. S8, and Fig. S9.

S9. Buckling transition – Numerical calculations of DNA extension and torque from the Marko model.

To describe the buckling transition, we follow the phase-coexistence formulation laid out by Marko[17]. Below, we separately outline the three phases of DNA below based on the Marko model: the pure stretched (or extended) state, and the pure plectonemic state, and the mixed state containing both stretched DNA and plectonemic DNA.

(1) Pure stretched state.

For DNA in a pure stretched state, the free energy per unit length is

$$E_{\text{s}}(F, \sigma) = -g(F) + \frac{kT\omega_0^2 C_{\text{eff}}(F)}{2} \sigma^2, \tag{S27}$$

where g is the energy of a nicked DNA under force, and $\omega_0 = \frac{2\pi}{h} = 1.77$ nm^{-1} is the conversion factor from the helical pitch of DNA to helical rotation. At the high force regime, g may be simplified by only considering the first two terms in the high-force expansion of the free energy of a semiflexible polymer[17]:

$$g(F) = F - \sqrt{\frac{k_B T F}{A}}. \tag{S28}$$

Although this expression is commonly used, it deviates significantly from the exact solution at the low force regime. We instead use a more accurate variational method[14] to calculate $g(F)$:

$$g(F) = -\min_a \left[\left(\frac{a k_B T}{2A} - F\right)\left(\coth 2a - \frac{1}{2a}\right)\right]. \tag{S29}$$

In particular, for the special case of DNA under no torsion, the force-extension relation can also be obtained from $g(F)$:

$$\frac{z(F,0)}{L} = \frac{dg(F)}{dF}. \tag{S30}$$

Fig. S2 compares predictions of the force-extension curve in the low force regime from different models. We found that the force-extension relation of the Marko model obtained using $g(F)$ from the variational method (Eq. S29) is nearly identical to our numerical solution of the force-extension relation of the BM model (Eq. S16) or to the Bouchiat model (Eq. S24) (Fig. S2). On the other hand, the force-extension relation of the MS interpolation model (Eq. 23) predicts forces that are ~ 10% higher than the more accurate models, while the Marko model using $g(F)$ from the high force approximation (Eq. S28) predicted forces much higher than the more accurate model.

When the DNA is under torsion, we use $C_{\mathrm{eff}}(F)$ from the modified-MN model for comparison with data taken at $F \geq 0.3$ pN, since there is a good agreement between measured $C_{\mathrm{eff}}(F)$ and

the modified-MN model in this force regime while the modified-MN model has a simple analytical expression. Therefore, the DNA extension is:

$$\frac{z(F,\sigma)}{L} = -\frac{\partial E_{\mathrm{S}}}{\partial F} = \frac{z(F,0)}{L} - \frac{1}{16}\omega_0^2\sigma^2C^2\left(\frac{k_{\mathrm{B}}T}{FA}\right)^{3/2}, \tag{S31}$$

The torque is:

$$\tau(F,\sigma) = \frac{\partial E_{\mathrm{S}}}{\partial \sigma} = kT\omega_0^2C_{\mathrm{eff}}\sigma = k_{\mathrm{B}}T\omega_0^2C\left(1 - \frac{C}{4A}\sqrt{\frac{k_{\mathrm{B}}T}{AF}}\right)\sigma. \tag{S32}$$

(2) Pure plectonemic state.

For DNA in a pure plectonemic state, the free energy per unit length is[18]:

$$E_{\mathrm{P}}(\sigma) = kT\omega_0^2\left(\frac{P_2}{2}\sigma^2 + \frac{P_3}{3}\sigma^3 + \frac{P_4}{4}\sigma^4\right). \tag{S33}$$

The P_2, P_3 and P_4 are the "persistence lengths" of the 2nd, 3rd and 4th order terms, respectively. This expression takes into consideration of possible anharmonicity in the free energy. For a harmonic plectonemic potential, $P_3 = P_4 = 0$, and $P_2 = P$. Because pure plectonemic DNA has zero extension $z = 0$, $E_{\mathrm{P}}(\sigma)$ does not depend on force. The torque is:

$$\tau(\sigma) = \frac{dE_{\mathrm{P}}}{d\sigma} = kT\omega_0^2(P_2\sigma + P_3\sigma^2 + P_4\sigma^3) \tag{S34}$$

(3) Mixed state with both stretched DNA and plectonemic DNA.

Based on Marko's phase-coexistence model[17], the free energy of DNA in a mixed state of stretched DNA and plectonemic DNA can be written as

$$E(F,\sigma) = x_{\mathrm{S}}E_{\mathrm{S}}(F,\sigma_s) + x_{\mathrm{P}}E_{\mathrm{P}}\left(F,\sigma_{\mathrm{P}}\right), \tag{S35}$$

where the E is the free energy of DNA of unit length, and x_{S} and x_{P} are the fractions of DNA in the stretched state and the plectonemic state, respectively. σ_{S} and σ_{P} are the σ values of the stretched and plectonemic DNA in the mixed state, respectively. They also correspond to the σ

values at the beginning and the end of the transition from the stretched state to the plectonemic state, respectively. These values are constant through the entire process of the phase transition process at a given force.

To find the buckling transition σ_{s}, the energy in Equation S35 is minimized under two constraints:

$$x_{\mathrm{s}} + x_{\mathrm{p}} = 1. \tag{S36}$$

$$x_{\mathrm{s}}\sigma_{\mathrm{s}} + x_{\mathrm{p}}\sigma_{\mathrm{p}} = \sigma, \tag{S37}$$

where σ can be an arbitrary value as long as the DNA is in the mixed, phase coexistence state.

For the harmonic model of plectonemic DNA, $\sigma_{\mathrm{s}}(F)$ has an analytical expression:

$$\sigma_s(F) = \frac{1}{C_{\mathrm{eff}}(F)}\sqrt{\frac{1}{k_{\mathrm{B}}T\omega_0^2}}\sqrt{\frac{2Pg(F)}{1-P/C_{\mathrm{eff}}}}. \tag{S38}$$

For the anharmonic model of plectonemic DNA, there is no analytical expression for σ_{s}, and numerical calculation is required to solve for σ_{s} using Eq. S36 and Eq. S37. After eliminating x_{p} and σ_{p}, the energy in Eq. S35 is minimized with respect to x_{s} and σ_{s} using the Nelder-Mead method to find the numerical solution of $x_{\mathrm{s}}(F,\sigma)$ and $\sigma_{\mathrm{s}}(F)$. Subsequently, $x_{\mathrm{p}}(F,\sigma)$ and $\sigma_{\mathrm{p}}(F)$ are also obtained.

For our work, we obtain $\sigma_{\mathrm{s}}(F)$ using $g(F)$ from the variational method (Eq. S29). We find that using this form of $g(F)$ is especially important at low forces (Fig. S3). Fig. S3 also suggests a minimum value of $\sigma_{\mathrm{s,min}}$~0.12, although this model may not be valid at the low force regime. Nonetheless, this is in line with an earlier study by Marko and Siggia that suggests $\sigma_{\mathrm{s,min}} =$ 0.02, below which the plectonemic state ceases to exist[19].

In the mixed state of stretched and plectonemic DNA, the extension of the DNA is proportional to the fraction of the stretched DNA, since plectonemic DNA has zero extension:

$$\frac{z(F,\sigma)}{L} = \frac{\sigma_{\mathrm{p}}-\sigma}{\sigma_{\mathrm{p}}-\sigma_{\mathrm{s}}}\frac{z(F,\sigma_{\mathrm{s}})}{L}. \quad \text{(S39)}$$

The torque remains constant for a given force.

$$\tau(F) = kT\omega_0^2 C_{\mathrm{eff}}(F)\sigma_{\mathrm{s}}. \quad \text{(S40)}$$

Note that Eq. S39 and Eq. S40 are used in Fig. 3, Fig. S8, and Fig. S9.

S10. Plectoneme torque measurement uncertainty

Ideally, the torque required to twist a DNA molecule in a pure plectoneme state should be measured at zero extension ($z = 0$). However, for reasons that we have provided in the main text, we measured the torque at a finite extension of $z = 500$ nm in Fig. 3a. Although the predominant contribution to the measurements is from the plectonemic state of the DNA, there is also some contribution from the extended DNA. To evaluate how well torque measurements at $z = 500$ nm reflect the desired torque at $z = 0$, we have performed the following analysis.

Consider the free energy of the DNA $E(z,\theta)$ which is a function of extension z and twist angle θ. Our desired free energy is $E(0,\theta)$ for a pure plectonemic state, while our measurements were carried out at a finite z. Here we estimate the contribution of the stretch DNA to the measured energy. Because $E(z,\theta)$ is a state function, the change in $E(z,\theta)$ is path independent. Thus $E(0,\theta)$ can be calculated by integrating along the path shown in Fig. S7a:

$$E(0,\theta) = \int_0^z F(z',0)dz' + \int_0^\theta \tau(z,\theta')d\theta' - \int_0^z F(z',\theta)dz'. \quad \text{(S41)}$$

It is also reasonable to assume that at a given θ, force monotonically increases with extension, i.e., $\frac{\partial F(z,\theta)}{\partial z} > 0$, and force is always greater than zero. Thus,

$$0 < \int_0^z F(z',\theta)dz' < zF(z,\theta). \quad \text{(S42)}$$

Therefore, the upper and lower bounds of $E(0,\theta)$ are:

$$E(0,\theta) < \int_0^z F(z',0)dz' + \int_0^\theta \tau(z,\theta')d\theta' = E_{\text{upper}}(0,\theta). \quad \text{(S43)}$$

$$E(0,\theta) > \int_0^z F(z',0)dz' + \int_0^\theta \tau(z,\theta')d\theta' - zF(z,\theta) = E_{\text{lower}}(0,\theta). \quad \text{(S44)}$$

Following the properties of an exact differential, the torque at $z = 0$ is related to the torque at $z = 500$ nm via the Maxwell relation,

$$\tau(0,\theta) = \tau(z,\theta) - \int_0^z \frac{\partial F(z',\theta)}{\partial \theta} dz'. \quad \text{(S45)}$$

Since the integral term is greater than zero, the upper bound is thus determined by:

$$\tau(0,\theta) < \tau(z,\theta) = \tau_{\text{upper}}(0,\theta). \quad \text{(S46)}$$

Based on the observation that $\frac{\partial F(z,\theta)}{\partial \theta}$ increases monotonically with z (Fig. 1b),

$$\int_0^z \frac{\partial F(z',\theta)}{\partial \theta} dz' < \frac{\partial F(z,\theta)}{\partial \theta} z, \quad \text{(S47)}$$

and thus the lower bound can be determined by:

$$\tau(0,\theta) > \tau(z,\theta) - \frac{\partial F(z,\theta)}{\partial \theta} z = \tau_{\text{lower}}(0,\theta) \quad \text{(S48)}$$

As shown in Fig. S7, the upper and lower bounds of the torque span a narrow range, suggesting that the contribution from the extended DNA to the torque data is minimal.

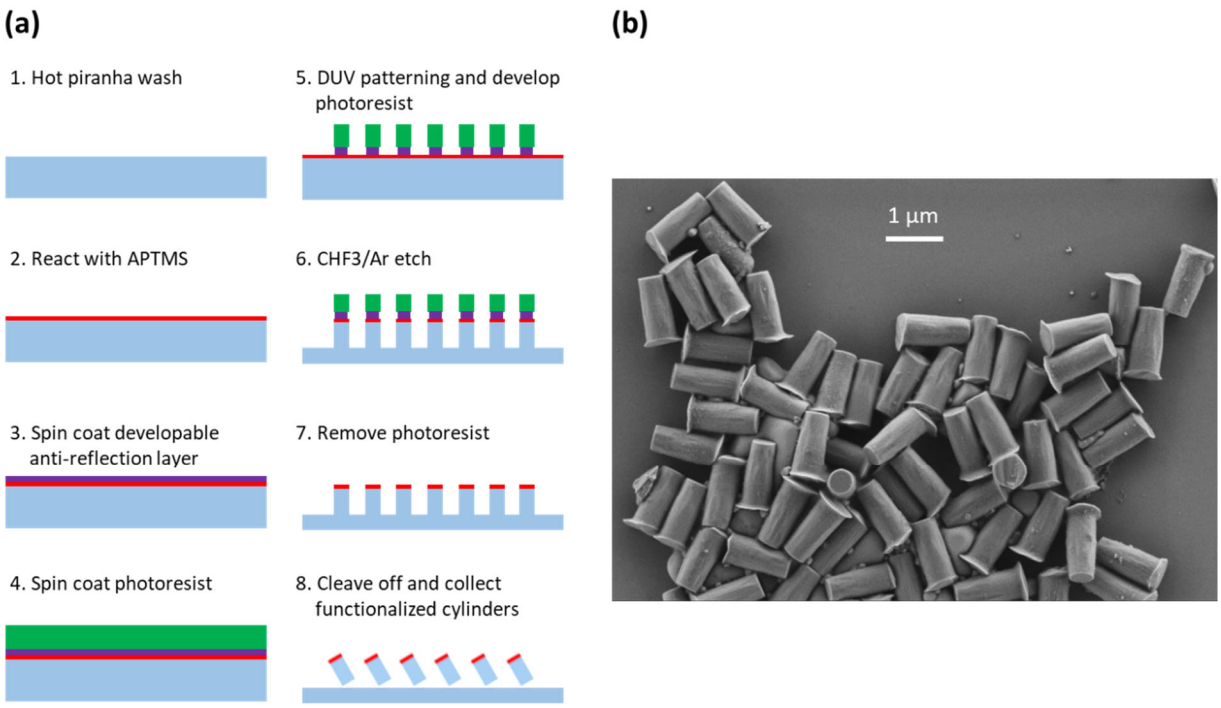

Figure S1. Nanofabrication of quartz cylinders. (a) Process flow for the fabrication process. For details, see SI Methods S3. (b) An SEM image of the cleaved cylinders.

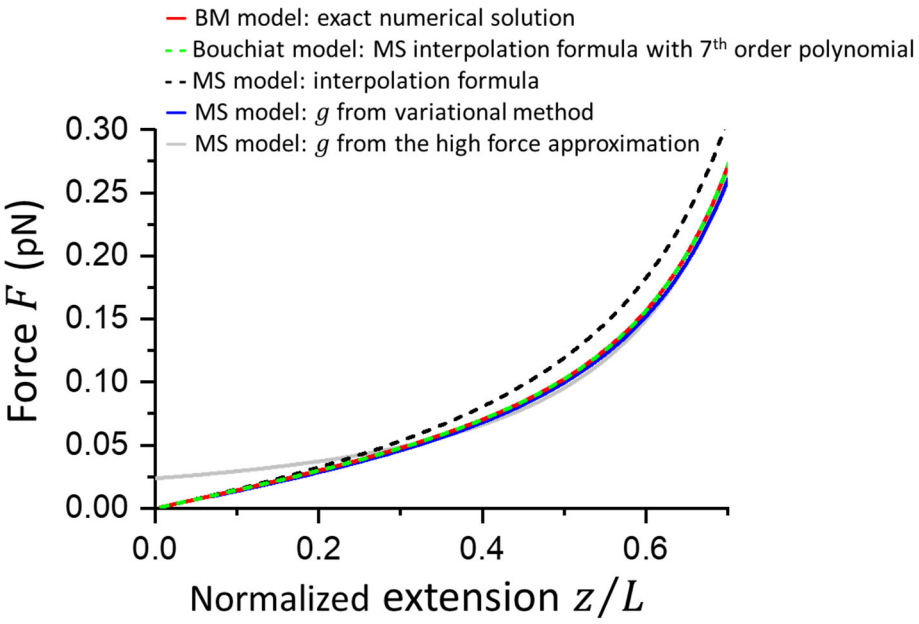

Figure S2. Comparison of predictions of the force-extension relations under no torsion in the low force regime by different models. For details, see Supplemental Methods S7 and S9. Red curve is from our numerical solution of the BM model (Eq. S16). Dotted green curve is from the Bouchiat model using a combination of the MS interpolation formula with a 7th order polynomial (Eq. S24) and is a good approximation for the BM model. The dotted black curve is the MS interpolation formula (Eq. S23). The blue curve is from our numerical solution of the MS model using the stretching energy $g(F)$ (Eq. S29) obtained from the variational method. The grey curve is the MS model using the stretching energy $g(F)$ (Eq. S28) obtained from the high force approximation. For all models, $A = 43$ nm.

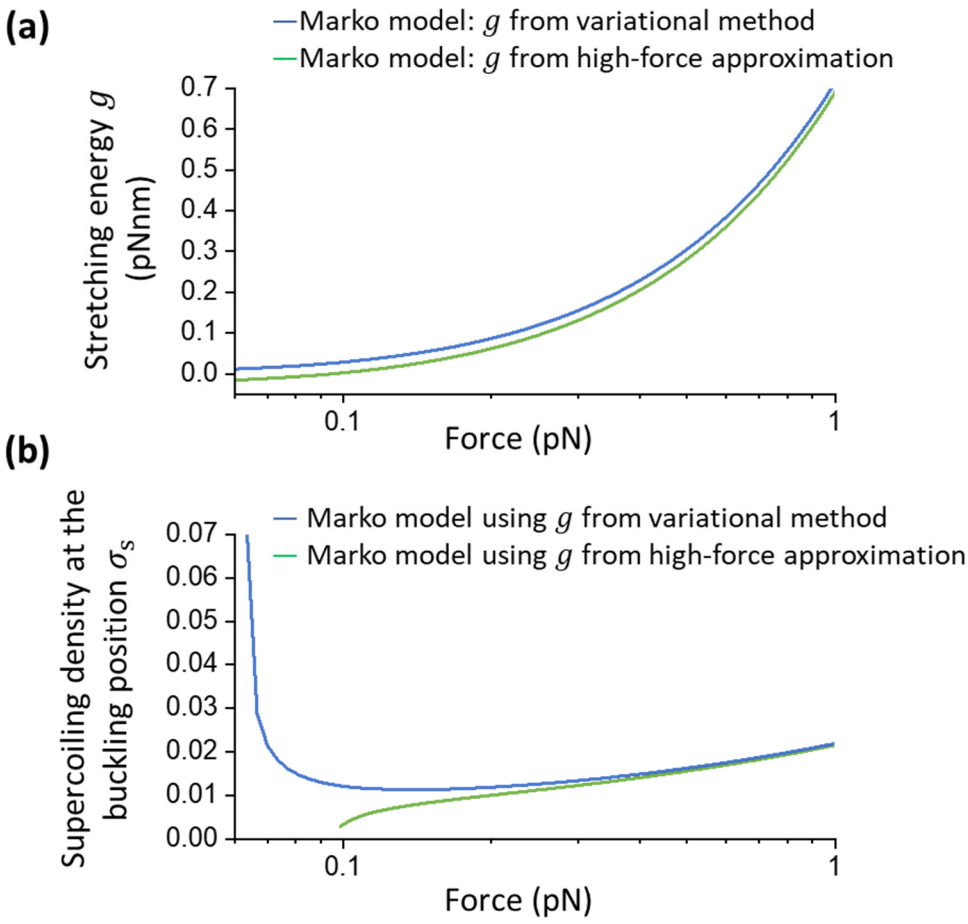

Figure S3. Predictions of the DNA buckling transition using the stretching energy $g(F)$ obtained via the high approximation or the variational method. (a) Comparison of $g(F)$ from the two formulations. (b) Comparison of the predicted supercoiling density at the buckling transition σ_s using these two formulations. Note that two curves differ significantly at the low force regime.

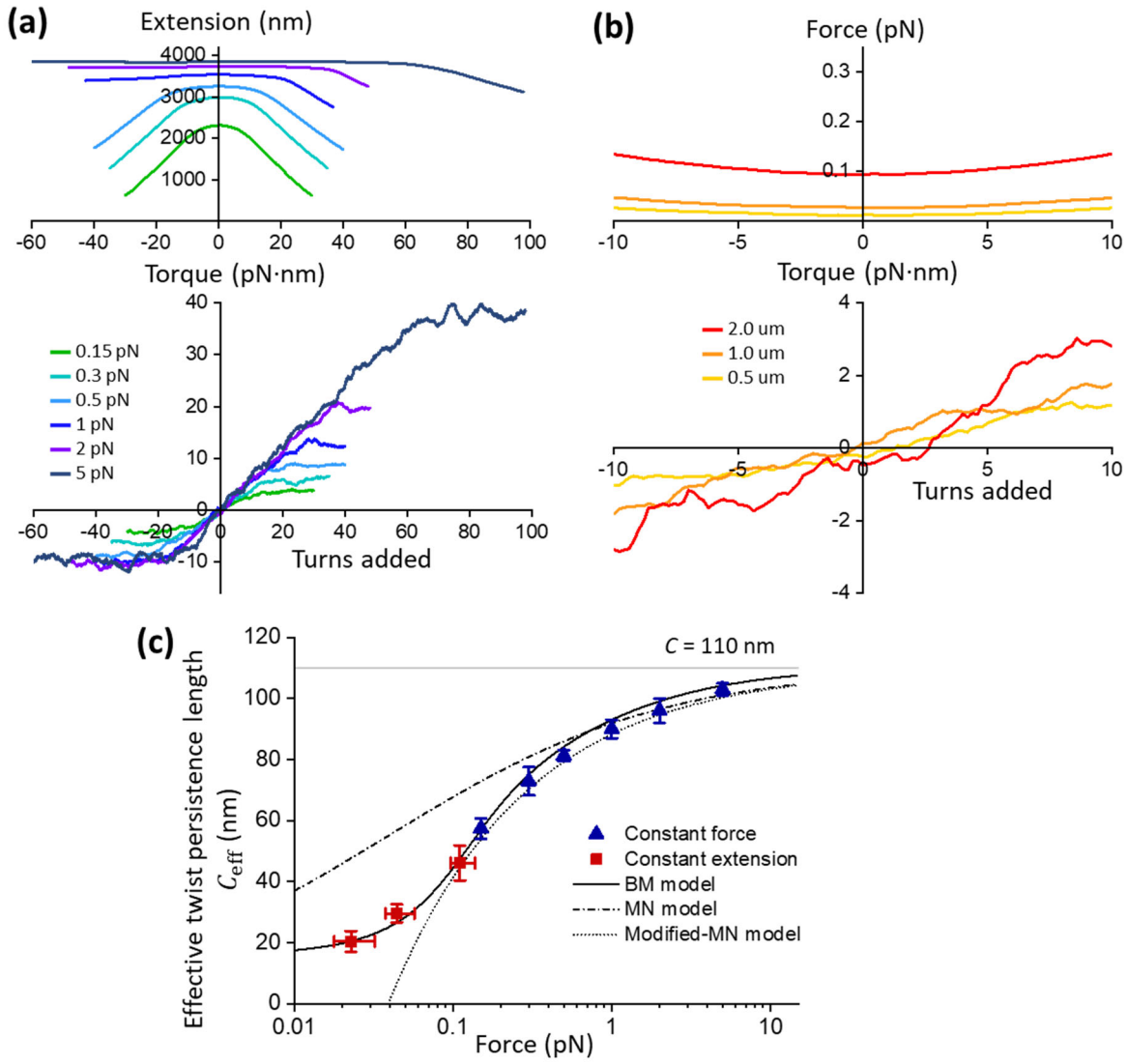

Figure S4. Experimental data and theoretical predictions of the torsional behavior of a 12,688 bp DNA which has a sequence different from that of the DNA template used in the main text. We repeated all the measurements shown in Fig. 1 and Fig. 2 of the main text using this template and found that the measurements were essentially unchanged. (a) Extension and torque versus turns measured under different constant forces. The data at 0.5 pN were from our previous study[1]. (b) Force and torque versus turns measured under different constant extensions. (c) The effective twist persistence length C_{eff} obtained from both the constant-force

and constant-extension experiments. The measured C_{eff} values at $F \geq 0.3$ pN were fit to the modified-MN model, yielding $C = 110$ nm. Using this C value, we plotted predictions of the BM model and the MN model for comparison. Note that these data are entirely consistent with those presented in Fig. 1 and Fig. 2.

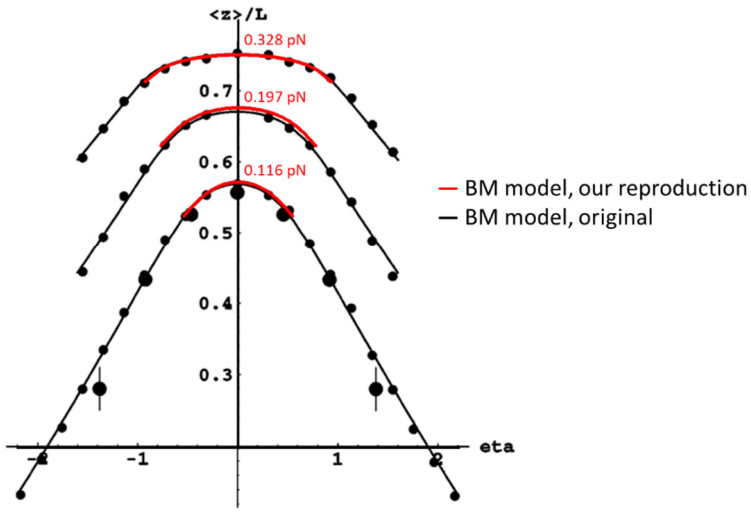

Figure S5. Comparison of hat curves from our reproduction of the BM model and from the original BM model. We calculated the hat curves using the same parameters as those used in Fig. 1 of the original BM model[12]. The forces of these curves (bottom to top) are 0.116, 0.197, and 0.328 pN, respectively. Plotted are hat curves of normalized DNA extension versus reduced supercoiling angle $\eta = 2\pi NA/L$, where N, A, and L are the linking number, bending persistence length, and DNA contour length, respectively. Adapted from Reference [12] with permission.

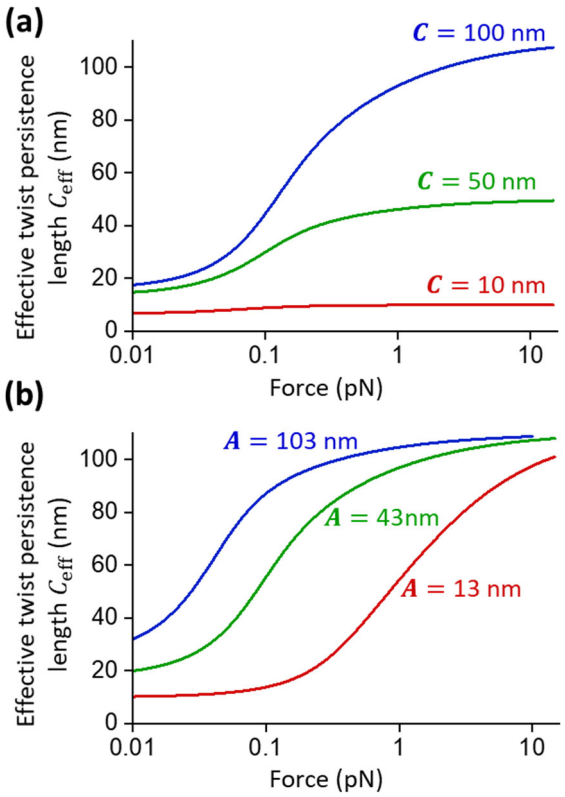

Figure S6. The effective torsional stiffness $C_{\mathrm{eff}}(F)$ based on our numerical calculation of the BM model.. (a) C_{eff} versus F at various values of C at a given $A = 43$ nm. For all curves, $b = 0.14A$ = 6.02 nm (b) C_{eff} versus F at various values of A at a given C =110 nm. For all curves, $b = 0.14A$.

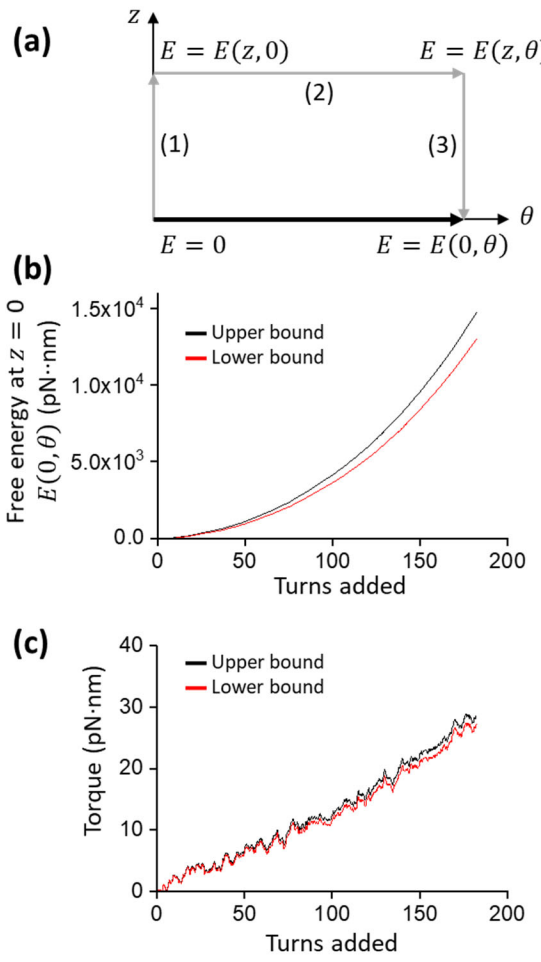

Figure S7. Estimating upper and lower bounds of the free energy and torque of pure plectonemic DNA using measurements from Fig. 3a. See Supplemental Methods S10 for details. (a) Path independence. To calculate the free energy of plectonemic DNA (the black path), the total free energy is integrated along the three segments of the gray path. (b) The lower and upper bounds of the free energy of pure plectonemic DNA estimated from the nonzero constant-extension experiment. (b) The lower and upper bounds of the torque of pure plectonemic DNA estimated from the nonzero constant-extension experiment. Note that the contribution to the measured torque from the stretched DNA state is rather small.

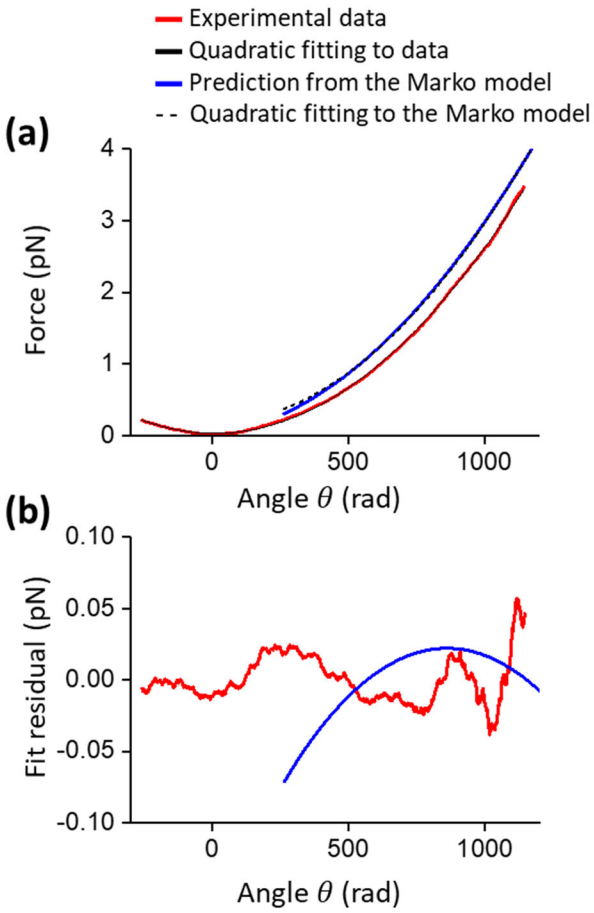

Figure S8. Analysis of the force-turns relation of the constant extension experiment (Fig. 3a). (a) A parabolic fit to the force-turns relation: $F(\theta) = a_o + a_2\theta^2$. For the measured relation, the fit yields $a_o = 0.026$ pN and $a_2 = 2.6 \times 10^{-6}$ pN. The coefficients are used to determine the $\partial F/\partial\theta$, in order to estimate the upper and lower bounds of the torque and free energy of plectonemic DNA(Supplemental Methods S10; Fig S7). For the predicted relation by the Marko model, the fit yields $a_o = 0.18$ pN and $a_2 = 2.8 \times 10^{-6}$ pN. (b) The residual force of the fits for the measured and predicted force-turns relations. Note that residuals are very small for both cases, indicating excellent fits.

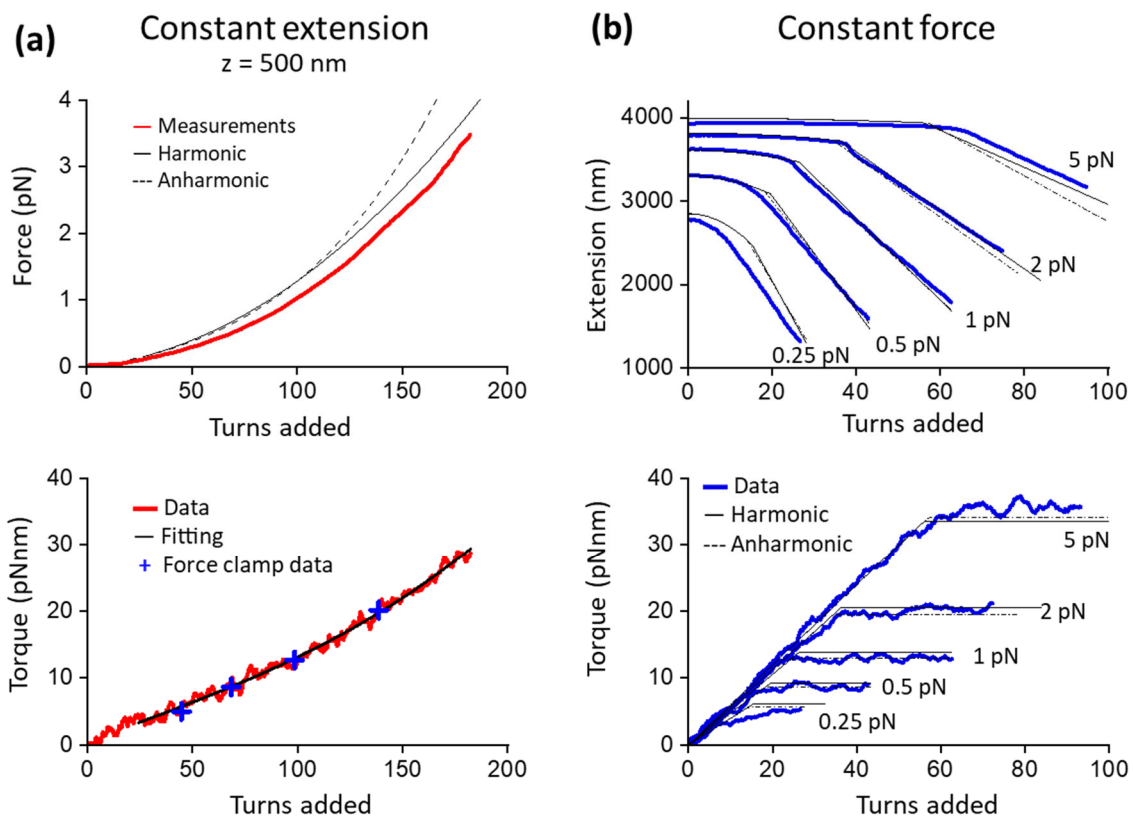

Figure S9. Comparison of predictions of the Marko model using a harmonic and anharmonic plectonemic energy. We replotted Figure 3, and overlaid predictions from the Marko model using an anharmonic plectonemic energy in order to directly compare with those from the Marko model using a harmonic plectonemic energy. (a) Constant extension data. We refit the torque-versus turns data with a 3rd order polynomial (Eq. S34). The coefficients of the anharmonic plectoneme free energy obtained from the fit are P_2 = 22.6 nm, P_3 = -52.9 nm, and P_4 = 541 nm. The intercept of the fitting function was fixed at zero. These parameters were used for predictions of the Marko model using an anharmonic plectonemic energy (black dashed curve). (a) Constant force data. We added the predictions from the Marko model using an anharmonic plectonemic energy to these plots.

References

[1] T. T. Le *et al.*, Cell **179**, 619 (2019).
[2] C. Deufel, S. Forth, C. R. Simmons, S. Dejgosha, and M. D. Wang, Nature Methods **4**, 223 (2007).
[3] A. La Porta and M. D. Wang, Physical Review Letters **92** (2004).
[4] J. Inman, S. Forth, and M. D. Wang, Optics Letters **35**, 2949 (2010).
[5] M. D. Wang, H. Yin, R. Landick, J. Gelles, and S. M. Block, Biophys J **72**, 1335 (1997).
[6] S. Forth, C. Deufel, M. Y. Sheinin, B. Daniels, J. P. Sethna, and M. D. Wang, Physical Review Letters **100** (2008).
[7] M. Y. Sheinin, S. Forth, J. F. Marko, and M. D. Wang, Physical Review Letters **107** (2011).
[8] M. Y. Sheinin and M. D. Wang, Physical Chemistry Chemical Physics **11**, 4800 (2009).
[9] J. Ma, L. Bai, and M. D. Wang, Science **340**, 1580 (2013).
[10] J. Ma, C. Tan, X. Gao, R. M. Fulbright, Jr., J. W. Roberts, and M. D. Wang, Proc Natl Acad Sci U S A **116**, 2583 (2019).
[11] C. Bouchiat, M. D. Wang, J. F. Allemand, T. Strick, S. M. Block, and V. Croquette, Biophys J **76**, 409 (1999).
[12] C. Bouchiat and M. Mezard, Physical Review Letters **80**, 1556 (1998).
[13] C. Bouchiat and M. Mezard, Eur Phys J E **2**, 377 (2000).
[14] J. F. Marko and E. D. Siggia, Macromolecules **28**, 8759 (1995).
[15] J. D. Moroz and P. Nelson, Proc Natl Acad Sci U S A **94**, 14418 (1997).
[16] J. D. Moroz and P. Nelson, Macromolecules **31**, 6333 (1998).
[17] J. F. Marko, Phys Rev E Stat Nonlin Soft Matter Phys **76**, 021926 (2007).
[18] J. F. Marko, in *Mathematics of DNA Structure, Function and Interactions*, edited by C. J. Benham. *et al.*2009), pp. 225.
[19] J. F. Marko and E. D. Siggia, Science **265**, 506 (1994).